Hindawi Publishing Corporation
Mathematical Problems in Engineering
Volume 2016, Article ID 3728397, 15 pages
http://dx.doi.org/10.1155/2016/3728397

Research Article

An Ultra-Low Frequency Two DOFs' Vibration Isolator Using Positive and Negative Stiffness in Parallel

Min Wang, Xuedong Chen, and Xiaoqing Li

The State Key Laboratory of Digital Manufacturing Equipment and Technology, Huazhong University of Science and Technology, Wuhan, Hubei, China

Correspondence should be addressed to Xiaoqing Li; xqli@hust.edu.cn

Received 26 July 2016; Revised 27 October 2016; Accepted 3 November 2016

Academic Editor: Roland Hildebrand

With the improvement of performance in the ultra-precision manufacturing engineering, the requirements for vibration isolation have become increasingly stringent. In order to get wider effective bandwidth and higher performance of vibration isolation in multiple DOFs system, an ultra-low frequency two DOFs' vibration isolator with positive and negative stiffness in parallel (PNSP) is proposed. The two DOFs' isolator which combines a positive stiffness (PS) air spring with a negative stiffness (NS) magnetic spring in parallel and combines a PS flat spring with an NS inverted pendulum in parallel is designed to reduce the natural frequency and broaden the effective bandwidth in horizontal and vertical direction. Based on this structure, stiffness models of different components in different directions are established. Compared with a PS isolator, it possesses the characteristic of high-static-low-dynamic stiffness. The simulation curves also provide strong evidence. Last, a real-time active control system and a spectrum testing and analysis system are used for the contrast experiment between the mentioned PNSP structure and PS only. The experimental results demonstrate that the isolator with PNSP can obviously reduce the natural frequency to 1 Hz and simultaneously maintain the stability of the system and consequently verify the validity and superiority of the mentioned structure.

1. Introduction

With the improvement of performance in the ultra-precision manufacturing and measuring equipment, the requirements for vibration isolation have become increasingly stringent [1–3]. Due to these problems, an effective control mechanism or a new structure is required to attenuate the vibration in order to preserve structural integrity of such systems [4]. An ultra-precision vibration isolation system with high performance has to break the routine to meet the strict requirements. The new system with low natural frequency and efficient active control technology is put forward to realize multi-degree of freedom (DOF) vibration isolation and wide effective bandwidth.

Absolute velocity feedback control can create a "sky-hook" damping to reduce the amplitude of resonance peak effectively without compromising high frequency performance [5]. Feedforward control shows a significant effect by predicting in advance against the vibration of the base platform and direct disturbance of the machine. It can effectively improve the performance of vibration isolation system [6, 7]. However, the realization of ultra-low frequency still depends on the design of passive structure.

Low stiffness can effectively reduce the natural frequency of the vibration isolation system and broaden the effective bandwidth of vibration isolation system. However, low stiffness is more likely to lead to instability of the vibration isolation system. Platus [8] from Minus K proposed a negative stiffness mechanism (NSM) based on the buckling of prestressed bars, and a vibration isolation system using the NSM was designed to obtain a lower natural frequency. Fulcher et al. [9] investigate the bistability and negative stiffness of a buckled beam mechanism in the vibration and shock isolation systems. Mizuno [10, 11] puts forward a novel isolator which combines a kind of zero power control NS magnetic spring with a PS spring in series. It shows a good aspect to resist the effect of vibration isolation directly on the payload direct disturbance but not quite fit the base vibration.

Under the condition that the carrying capacity is constant, the continuous reduction of the stiffness will lead

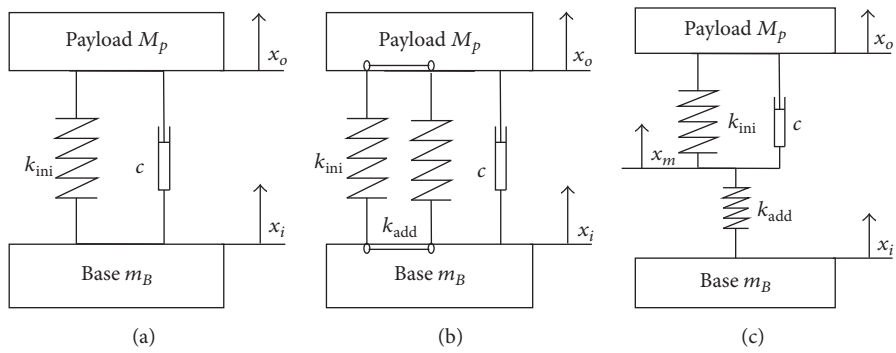

Figure 1: Vibration isolation principle diagram: (a) traditional, (b) stiffness in parallel, and (c) stiffness in series.

to the formation of quasi-zero-stiffness (QZS) system [12–15]. QZS mechanisms are generally achieved by combining a negative stiffness (NS) element with a positive stiffness (PS) element. It has been found that, to achieve a large excursion from the static equilibrium position such that the stiffness of the system does not exceed a prescribed value, there is an optimum geometry and a corresponding optimum relationship in the stiffness [14].

Based on QZS system, Carrella et al. [14, 16] put forward the concept of the high-static-low-dynamic stiffness (HSLDS) mount which comprises two vertical mechanical springs and a permanent magnet. A reduction in the natural frequency from 14 Hz to 7 Hz was achieved by using the magnets, and the measured transmissibility from a displacement input showed that the device behaved approximately linearly. Robertson et al. [12] introduced theoretical analysis for a fully HSLDS magnetic spring for vibration isolation, where the payload was also supported by magnetism. Shaw et al. [17] presented dynamic analysis of HSLDS vibration isolation mounts to provide useful insight into the design of HSLDS mounts. However, there are some problems in the existing vibration isolators based on the efforts of QZS and HSLDS. Specific performances are as follows: the natural frequency of existed structure is still not competitive, when faced with a higher demand. There are still some shortcomings in the application of multi-DOFs vibration isolation system. Therefore, one structure of urgent demands to solve these problems is becoming more and more necessary.

In this paper, to get wider effective bandwidth and higher performance of vibration isolation in multiple DOFs system, an ultra-low frequency two DOFs' vibration isolator with positive and negative stiffness in parallel (PNSP) is proposed, which can realize this requirement that ensures lower natural frequency and large capacity at the same time [12] and the function that isolation can be achieved simultaneously in two DOFs. Compared with a PS isolator, it can also possess the characteristic of HSLDS. The ultra-low frequency two DOFs' isolator which combines a PS air spring with a NS magnetic spring in parallel and combines a PS flat spring with an NS inverted pendulum in parallel is designed to reduce the natural frequency and broaden the effective bandwidth in horizontal and vertical direction. The bearing capacity is determined by the PS structure which can effectively improve the static stiffness and the stability of the vibration system and maintain the natural frequency which is constant with the changing of payload. NS element is employed to reduce the dynamic stiffness and the natural frequency of vibration system.

To solve the problem of the existence of vibration isolation in multi-DOFs at the same time, three identical vibration isolators proposed in this paper can be used together to establish an ultra-precision vibration isolation system which can realize the ultra-low frequency vibration isolation in six DOFs through the transform matrix of different coordinate systems in this paper. And it also can ensure the positioning accuracy of the system simultaneously.

2. Design of Two DOFs' Ultra-Low Frequency Vibration Isolator

2.1. The Principle of PNSP. The traditional passive vibration isolation unit is composed of mass-spring-damping; the simplified principle diagram is shown in Figure 1(a). Common ways of changing the system stiffness are the method of series connection or parallel connection with additional stiffness; Figures 1(b) and 1(c) show the simplified principle diagram.

The way of series can only reduce the system stiffness, but it cannot achieve the QZS system. This can be improved upon by incorporating a negative stiffness element in parallel such that the dynamic stiffness is much less than the static stiffness. The way to achieve this result of high-static stiffness and low-dynamic stiffness is that the negative stiffness element is added near the working position of the isolator to form the PNSP mechanism.

According to Newton-Euler equation, the dynamic mathematical equations of the vibration isolation system with traditional passive vibration isolation and with additional stiffness in parallel are, respectively, written as

$$M_p\ddot{x}_o + c\left(\dot{x}_o - \dot{x}_i\right) + k_{\text{ini}}\left(x_o - x_i\right) = 0, \tag{1}$$

$$M_p\ddot{x}_o + c\left(\dot{x}_o - \dot{x}_i\right) + k_{\eta}\left(x_o - x_i\right) = 0, \tag{2}$$

where M_p is the mass of payload platform, m_B is the mass of base platform, c is the equivalent damping of the system, x_o is the displacement deformation of the payload platform, x_i

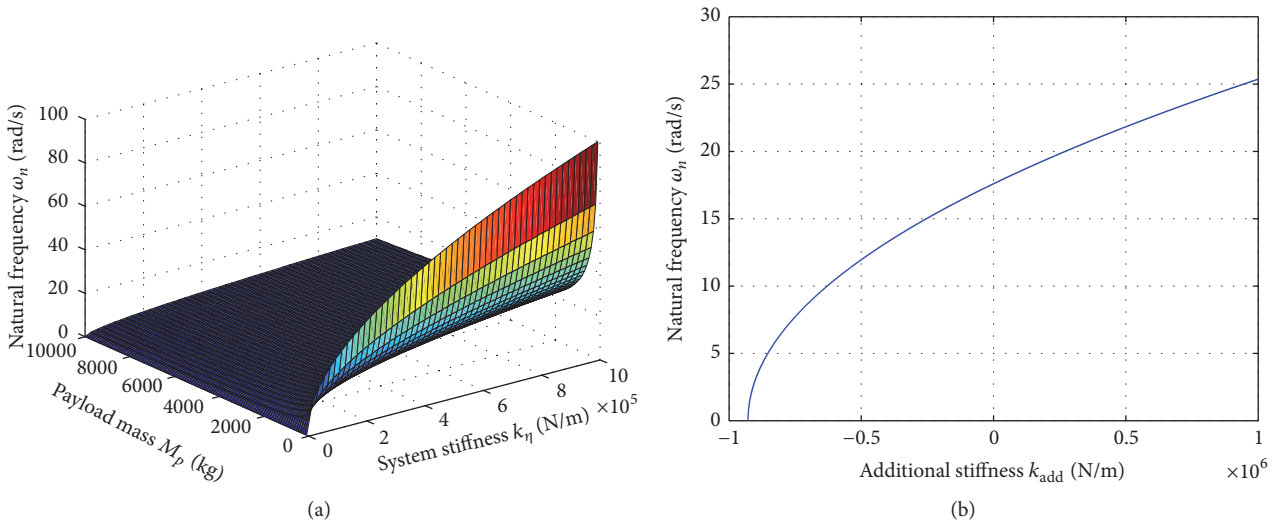

FIGURE 2: The simulation curves, (a) the relationship between system stiffness ($k_\eta \in (0, 1e6)$ N/m), payload mass ($M_p \in (0, 1e4)$ kg), and natural frequency ω_n; (b) the relationship between additional stiffness ($k_{add} \in (0, 1e6)$ N/m) and natural frequency ω_n, when initial stiffness ($k_{ini} = 9.28e5$ N/m) and payload mass ($M_p = 3000$ kg) are constant.

is the displacement deformation of the base platform, k_η is the equivalent system stiffness after the change, and k_{ini} is the initial equivalent stiffness.

According to the principle of vibration system, the natural frequency of vibration isolation system has the following mathematical relations with the system stiffness and the system payload:

$$\omega_n = \sqrt{\frac{k_\eta}{M_p}} = \sqrt{\frac{k_{ini} + k_{add}}{M_p}} \tag{3}$$

$$k_{add} = M_p \omega_n^2 - k_{ini},$$

where ω_n is the natural frequency of vibration system and k_{add} is the additional stiffness.

Equation (3) is simulated and analyzed and is shown in Figure 2. As can be seen from Figure 2(a), the natural frequency of the system is obviously changed with the payload of the system (especially the initial payload mass segment), when the system stiffness is constant. Reducing the natural frequency can be achieved by means of enlarging the payload of the system and simultaneously maintaining low system stiffness. However, the payload cannot always increase. And in some cases, the payload is constant.

Figure 2(b) shows that the relationship between the natural frequency and the additional stiffness is nonlinear and similar to the inverse exponential curve, when the payload and initial stiffness are constant. The natural frequency is the trend of steep rise in the condition that the additional stiffness is from negative to zero; the natural frequency of the system is into the trend of slow rise trend in the condition that the additional stiffness is from zero to a greater positive. So when the negative stiffness is adopted as the additional stiffness, the lower the value is, the more obvious the change is, and the easier it is to form a quasi-zero stiffness system.

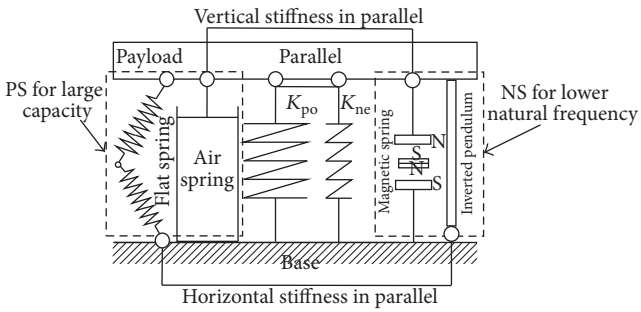

FIGURE 3: The structure sketch of passive isolator using PNSP.

2.2. The Structure of Two DOFs' Isolator. The frequency range over which a linear passive vibration isolator is effective is often limited by the mount stiffness required to support a static load. This can be improved upon by incorporating a negative stiffness element to form a high-static-low-dynamic stiffness mount, which can be approximated to achieve the quasi-zero stiffness system, and the structure sketch is shown in Figure 3.

According to the structure sketch of Figure 3, the schematic diagram of stiffness in parallel is proposed separately from the horizontal and vertical direction. The following can be seen from Figure 4.

In vertical direction, the structure which combines a PS air spring with a NS magnetic spring in parallel is mentioned. The PS air spring can support the mass of payload platform, and the NS magnetic spring is responsible for realizing ultra-low frequency vibration isolation. The stiffness of the system can be changed by adjusting the position of the middle magnet.

In horizontal direction, the structure which combines a PS flat spring with a NS inverted pendulum in parallel is used to attain ultra-low frequency vibration isolation. The NS

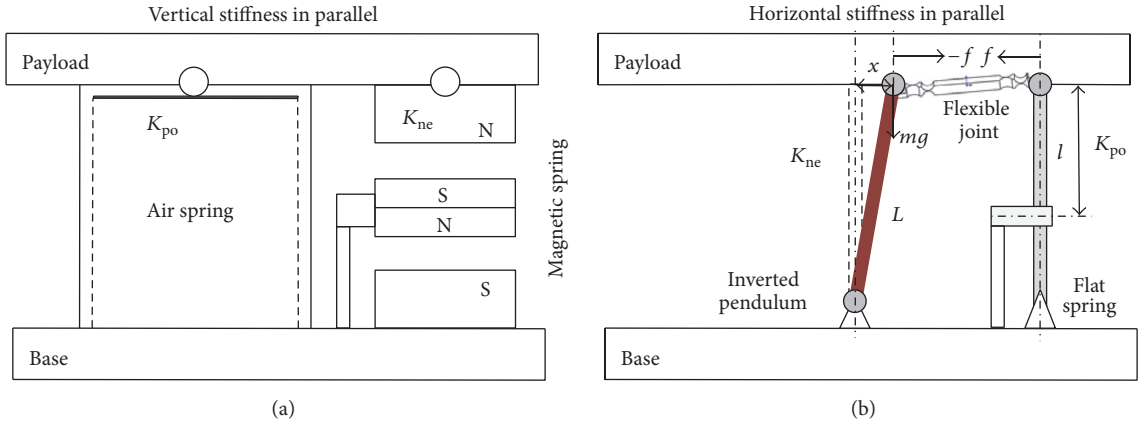

Figure 4: The schematic diagram of stiffness in parallel, (a) vertical direction; (b) horizontal direction.

inverted pendulum is realized through the reverse installing of the air spring. When the payload is very large (about 1000 kg), the cross-sectional area of the air spring is relatively small, which can be equivalent to simply supported beam structure. When one end of the simply supported beam is installed on the base platform and can be rotated, the other end is connected with the payload platform and also can be rotated. A pendulum structure that adopts inverted installation is formed.

At the same time, in order to eliminate the influence of the force from the other directions, a flexible joint with lower bending stiffness in the DOFs not required is adopted to serve for horizontal and vertical motion decoupling. A two DOFs' ultra-low frequency vibration isolator is set up.

After PNSP, the stiffness of horizontal and vertical direction can be expressed as

$$\begin{aligned} k_\eta^V &= K^V = K_{po}^V + K_{ne}^V = K_{as} + K_{ms}, \\ k_\eta^H &= K^H = K_{po}^H + K_{ne}^H = K_{fs} + K_{ip}, \end{aligned} \tag{4}$$

where $k_\eta^V = K^V$ is the system stiffness of vertical direction, K_{po}^V is the positive stiffness of vertical direction, K_{ne}^V is the negative stiffness of vertical direction, K_{as} is the stiffness of air spring, K_{ms} is the stiffness of magnetic spring, $k_\eta^H = K^H$ is the system stiffness of horizontal direction, K_{po}^H is the positive stiffness of horizontal direction, K_{ne}^H is the negative stiffness of horizontal direction, K_{fs} is the stiffness of flat spring, and K_{ip} is the stiffness of inverted pendulum.

3. Stiffness Model

3.1. Vertical Stiffness Model. In vertical direction, the structure combines a PS air spring with a NS magnetic spring in parallel. The PS air spring can support the mass of payload platform, and the NS magnetic spring is responsible for realizing ultra-low frequency vibration isolation.

3.1.1. PS Air Spring. A single chamber air spring is designed to be an inverted pendulum. The stiffness model is established to describe the dynamic characteristics of vertical passive vibration isolation element. The structure diagram is shown in Figure 5.

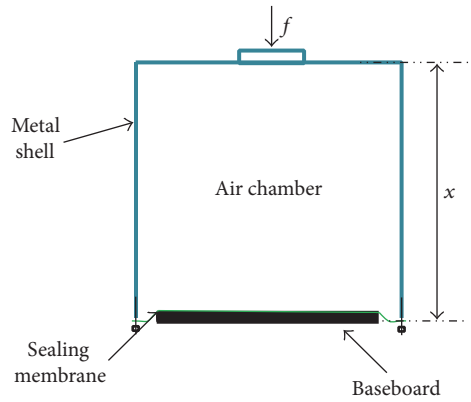

Figure 5: The structure diagram of air spring.

To establish stiffness model of the single chamber air spring shown in Figure 5, the dynamic process of metal cavity in the body is assumed as an ideal gas adiabatic process:

$$PV^\kappa = P_0 V_0^\kappa, \tag{5}$$

where P is the pressure of the air chamber, V is the volume of the air chamber, P_0 is the initial pressure of the air chamber under static equilibrium state, V_0 is the initial volume of the air chamber under static equilibrium state, κ is the adiabatic coefficient, and the value is about 1.402.

Under static equilibrium state of the air chamber, the initial volume and initial pressure satisfy the following mathematical relations:

$$\begin{aligned} P_0 &= P_{atm} + \frac{M_p g}{A}, \\ V_0 &= A x_0, \end{aligned} \tag{6}$$

where x_0 is the initial height of the air chamber, A is the effective sectional area of the air chamber, P_{atm} is the pressure

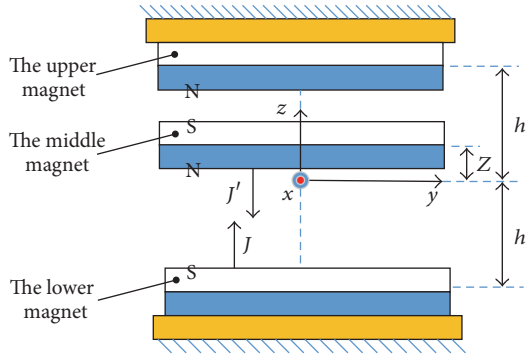

Figure 6: The schematic of NS magnetic spring.

of atmosphere, and M_p is the mass of payload under static equilibrium state.

When the amplitude of the air spring vibration is very small near the equilibrium position, the volume of air chamber can be approximately considered as constant. Equation (5) is differentiable at V *and is changed to*

$$\frac{dP}{dV} = -\kappa \frac{P_0}{V_0} \left(\frac{V_0}{V}\right)^{\kappa+1} \approx -\kappa \frac{P_0}{V_0}. \tag{7}$$

When there is an effect on payload from perturbation f, the volume and pressure of the air chamber meet the following relations:

$$\begin{aligned} AdP &= df, \\ dV &= Adx. \end{aligned} \tag{8}$$

According to the definition of stiffness and the above mathematical formulas, the stiffness of air spring can be derived as

$$K_{\text{as}} = -\frac{df}{dx} = \frac{\kappa A^2 \left(P_{\text{atm}} + M_p g/A\right)}{V_0}. \tag{9}$$

The positive stiffness of vertical direction is expressed as

$$K_{\text{po}}^V = K_{\text{as}} = \frac{\kappa A^2 \left(P_{\text{atm}} + M_p g/A\right)}{V_0}. \tag{10}$$

From (10), it can be seen that the stiffness of the single chamber air spring is related to the mass M_p of payload, the effective sectional area A of the air chamber, and the initial volume V_0 of the air chamber. With the increase of mass, the stiffness of air spring will also increase.

3.1.2. NS Magnetic Spring. The principle of NS magnetic attraction spring is that different magnetic poles can attract each other. The schematic is depicted in Figure 6. There are three rectangular magnets magnetized in the z-direction. The middle magnet and the upper/lower magnets are configured in attractive interaction. Due to the symmetry, the middle magnet maintains a balance in the expected initial position. But the balance is unstable. Once a small perturbation acts on it, the balance will be broken and cannot be restored without external force. Thus, the middle magnet acts as a NS spring [18].

It is assumed that the middle magnet can move only in the z-direction. The other degrees of freedom will be constrained by applying extra mechanism. As shown in Figure 6, the upper and the lower magnets are fixed with respect to each other. The distance of the outer magnet and the middle magnet in the z-direction is h. The stiffness of the magnetic spring attributes to magnetic force. It can be adjusted by changing the distance h between the central magnet and the outer magnets.

According to the research of rectangular permanent magnet magnetic force analytical model from [18], the resultant force of the middle magnet is from the effect of the upper and lower magnets in z direction

$$F_z = F(z-h) + F(z+h). \tag{11}$$

For the magnets shown in Figure 6, we can obtain the mathematical formula of attractive force between the two magnets from [19]

$$\begin{aligned} F = {} & \frac{JJ'}{4\pi\mu_0} \\ & \cdot \sum_{i=0}^{1}\sum_{j=0}^{1}\sum_{k=0}^{1}\sum_{l=0}^{1}\sum_{p=0}^{1}\sum_{q=0}^{1} (-1)^{i+j+k+l+p+q} \Phi\left(U_{ij}, V_{kl}, W_{pq}, r\right), \end{aligned} \tag{12}$$

where J and J' are the magnetic polarization vectors and the variables U, V, W, and r, respectively, are

$$\begin{aligned} \Phi\left(U_{ij}, V_{kl}, W_{pq}, r\right) = {} & -UW \ln(r-U) \\ & - VW \ln(r-V) \\ & + UV \arctan\left(\frac{UV}{rW}\right) - rW, \\ U_{ij} = {} & y + (-1)^j a' - (-1)^i a, \\ V_{kl} = {} & (-1)^l b' - (-1)^k b, \\ W_{pq} = {} & z + (-1)^q c' - (-1)^p c, \\ r = {} & \sqrt{{U_{ij}}^2 + {V_{kl}}^2 + {W_{pq}}^2}, \end{aligned} \tag{13}$$

where the geometric dimensions of the upper/lower magnets are $2a \times 2b \times 2c$ and the geometric dimensions of the middle magnet are $2a' \times 2b' \times 2c'$.

According to the definition of stiffness, the stiffness of NS magnetic spring is expressed as

$$K = -\frac{\partial F_z}{\partial z} = K(z-h) + K(z+h). \tag{14}$$

The mathematical expression of $K(z)$ is

$$K_{\mathrm{ms}}(z) = \frac{JJ'}{4\pi\mu_0} \cdot \sum_{i=0}^{1}\sum_{j=0}^{1}\sum_{k=0}^{1}\sum_{l=0}^{1}\sum_{p=0}^{1}\sum_{q=0}^{1}(-1)^{i+j+k+l+p+q}\varphi\left(U_{ij}, V_{kl}, W_{pq}, r\right) \tag{15}$$

with

$$\varphi\left(U_{ij}, V_{kl}, W_{pq}, r\right) = 2r + U\ln(r-U) + V\ln(r-V), \tag{16}$$

ditto the variables U, V, W, and r.

The negative stiffness of vertical direction is expressed as

$$K_{\mathrm{ne}}^{V} = K_{\mathrm{ms}} = \frac{JJ'}{4\pi\mu_0} \cdot \sum_{i=0}^{1}\sum_{j=0}^{1}\sum_{k=0}^{1}\sum_{l=0}^{1}\sum_{p=0}^{1}\sum_{q=0}^{1}(-1)^{i+j+k+l+p+q}\varphi\left(U_{ij}, V_{kl}, W_{pq}, r\right). \tag{17}$$

The stiffness of vertical direction can be derived as

$$K^{V} = K_{\mathrm{po}}^{V} + K_{\mathrm{ne}}^{V} = \frac{\kappa A^2\left(P_{\mathrm{atm}} + M_p g/A\right)}{V_0} + \frac{JJ'}{4\pi\mu_0} \cdot \sum_{i=0}^{1}\sum_{j=0}^{1}\sum_{k=0}^{1}\sum_{l=0}^{1}\sum_{p=0}^{1}\sum_{q=0}^{1}(-1)^{i+j+k+l+p+q}\varphi\left(U_{ij}, V_{kl}, W_{pq}, r\right). \tag{18}$$

3.2. Horizontal Stiffness Model. In horizontal direction, the structure which combines a PS flat spring with a NS inverted pendulum in parallel is used to attain ultra-low frequency vibration isolation. The NS inverted pendulum is realized through the reverse installing of the air spring.

3.2.1. PS Flat Spring. The horizontal PS structure is made up of two mutually perpendicular flat spring mechanisms. Every flat spring mechanism consists of two parallel flat springs which is rectangular.

Two mutually perpendicular flat spring mechanisms can be equivalent to Figure 7. In the figure, point A is the working point of force. When there is one unit force F from arbitrary direction (angle θ is arbitrary value) at point A, the flat spring will produce the static deformation to point B in the direction of F. The static deformation which is generated by component force of F in k_1 and k_2 direction is expressed as

$$\Delta x_1 = \frac{F\cos(45^\circ + \theta)}{k_1}, \qquad \Delta x_2 = \frac{F\cos(45^\circ - \theta)}{k_2}. \tag{19}$$

Assume that the unit force F is very small, so the static deformation is very small. Angle $\angle CBD$ is still approximately considered as the right angle; the total deformation Δx is indicated as

$$\Delta x = \sqrt{\Delta x_1^2 + \Delta x_2^2}. \tag{20}$$

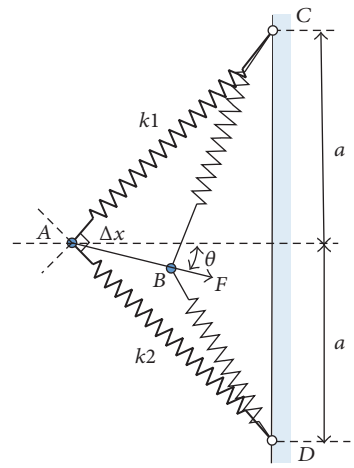

Figure 7: The schematic of two mutually perpendicular flat spring mechanisms.

The stiffness k_1 and stiffness k_2 are the same as the stiffness k of flat spring; the total stiffness of the mechanism in the direction of θ can be derived as

$$k_{hp} = \frac{F}{\Delta x} = \frac{F}{\sqrt{\left(F\cos(45^\circ+\theta)/k_1\right)^2 + \left(F\cos(45^\circ-\theta)/k_1\right)^2}} = k = 2k_s. \tag{21}$$

The stiffness of flat spring which is fixed at one end and freed on the other end can be expressed as

$$k_s = \frac{3EI}{L^3}, \tag{22}$$

where E is the elastic modulus of flat spring material, I is the bending section moment of inertia, and L is the effective bending length of flat spring.

The positive stiffness of horizontal direction is expressed as

$$K_{\mathrm{po}}^{H} = K_{\mathrm{fs}} = 2k_s = \frac{6EI}{L^3}. \tag{23}$$

Given the arbitrariness of angle θ, the stiffness of the mechanism is all consistent in arbitrary direction.

3.2.2. NS Inverted Pendulum. The structure of inverted pendulum is not a real pendulum. Instead, the inverted pendulum is formed by the inverted installation of air spring. Sealing membrane of air spring is fixed on the base platform. When there is a small perturbation effect on the inverted air spring, the special arrangement acts as a NS inverted pendulum. The equivalent structure chart is shown in Figure 8. A flexible joint is served for connective functions between the payload and the air spring. Owing to the flexible joint with low stiffness, the payload always keep in a horizontal state. Because of this reason, the connection of the vertical mechanism can be considered as rigid connection.

Under the undisturbed nature state, inverted pendulum is in the unstable equilibrium state. Once a small perturbation acts on it, the state cannot be restored. When there is a disturbance effect on payload, a horizontal movement x deviated from the original unstable equilibrium state will be produced. We need to make a balance on the displacement x by applying a reverse force f on this point. The reverse force f can be expressed as

$$f = -mg\frac{x}{\sqrt{l^2 - x^2}}. \tag{24}$$

According to the definition of stiffness, the mathematical formula about the stiffness of NS inverted pendulum is expressed as

$$k = \frac{df}{dx} = -mg\left(\frac{1}{\sqrt{l^2 - x^2}} + \frac{x^2}{\sqrt{\left(l^2 - x^2\right)^3}}\right). \tag{25}$$

Further, when the horizontal amplitude x is in a small range and it is far less than the effective length l, (25) can be rewritten as

$$k = -\frac{mg}{l}. \tag{26}$$

The negative stiffness of horizontal direction is expressed as

$$K_{\text{ne}}^H = K_{\text{ip}} = -\frac{mg}{l}. \tag{27}$$

From (27), it can be seen that the value of negative stiffness is related to the payload and the effective length of inverted pendulum, and the inverted pendulum is characterized by negative stiffness. However, the characteristic determines that inverted pendulum must be used with positive stiffness spring in parallel

The stiffness of horizontal direction can be derived as

$$K^H = K_{\text{po}}^H + K_{\text{ne}}^H = \frac{6EI}{L^3} - \frac{mg}{l}. \tag{28}$$

4. Numerical Simulation

4.1. Numerical Simulation of Stiffness Model. According to the above stiffness model, the simulation curves which give the relationship between the stiffness of different component and associated parameter values are shown in Figure 9.

From Figure 9(a), it can be seen that the stiffness of air spring will decrease with the increase of volume. This change is more obvious when the initial volume of the air chamber is small. As the value increases to a certain extent, the effect becomes less significant. It also shows that the stiffness of air spring with different payload mass shows the same change trend.

Figure 9(b) shows that the amplitude of the stiffness decreases as the relative displacement y increases within a certain vibration range, and it reaches the maximum when y equals zero. In particular, the stiffness also depends on the distance h, and it can be utilized to adjust the stiffness of the NS.

According to (26) and Figure 9(c), the value of the stiffness is inversely related to the effective bending length L. Therefore, the value of the stiffness can be affected and adjusted by the effective bending length.

The value of negative stiffness is related to the payload and the effective length of inverted pendulum, and the inverted pendulum is characterized by negative stiffness in Figure 9(d). However, the characteristic determines that inverted pendulum must be used with positive stiffness spring in parallel.

4.2. Numerical Simulation of Vibration Isolation System. According to Newton-Euler equation, the dynamic mathematical equations of the vibration isolation system with additional stiffness in parallel separately from the horizontal and vertical direction are changed as

$$\begin{aligned} M_p\ddot{x}_o + c^V\left(\dot{x}_o - \dot{x}_i\right) + \Bigg[&\frac{\kappa A^2\left(P_{\text{atm}} + M_p g/A\right)}{V_0} + \frac{JJ'}{4\pi\mu_0} \\ &\cdot \sum_{i=0}^{1}\sum_{j=0}^{1}\sum_{k=0}^{1}\sum_{l=0}^{1}\sum_{p=0}^{1}\sum_{q=0}^{1}(-1)^{i+j+k+l+p+q}\varphi\left(U_{ij}, V_{kl}, W_{pq}, r\right)\Bigg] \\ &\cdot\left(x_o - x_i\right) = 0, \\ M_p\ddot{x}_o + c^H\left(\dot{x}_o - \dot{x}_i\right) + &\left[\frac{6EI}{L^3} - \frac{mg}{l}\right]\left(x_o - x_i\right) = 0. \end{aligned} \tag{29}$$

The natural frequency with PNSP is put into

$$\begin{aligned} \omega_n^V &= \sqrt{\frac{k_\eta}{M_p}} \\ &= \sqrt{\frac{\kappa A^2\left(P_{\text{atm}} + M_p g/A\right)/V_0 + \left(JJ'/4\pi\mu_0\right)\sum_{i=0}^{1}\sum_{j=0}^{1}\sum_{k=0}^{1}\sum_{l=0}^{1}\sum_{p=0}^{1}\sum_{q=0}^{1}(-1)^{i+j+k+l+p+q}\varphi\left(U_{ij}, V_{kl}, W_{pq}, r\right)}{M_p}}, \\ \omega_n^H &= \sqrt{\frac{k_\eta^H}{M_p}} = \sqrt{\frac{6EI/L^3 - mg/l}{M_p}}. \end{aligned} \tag{30}$$

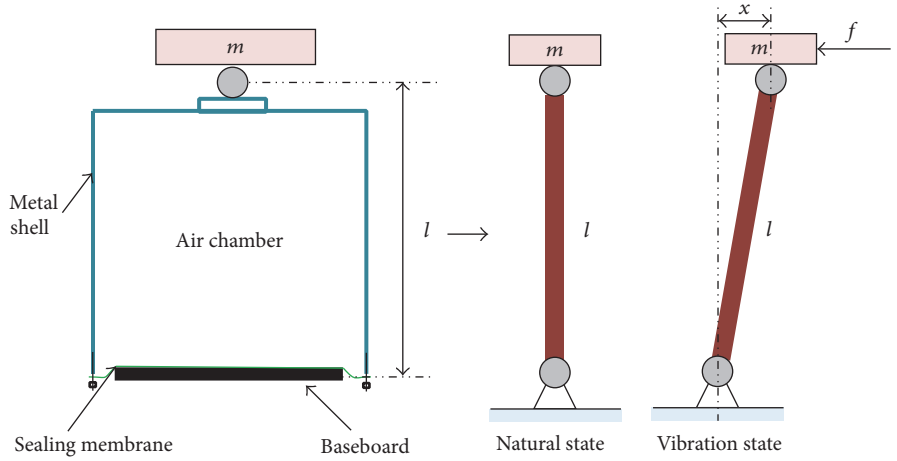

FIGURE 8: The equivalent structure chart of NS inverted pendulum.

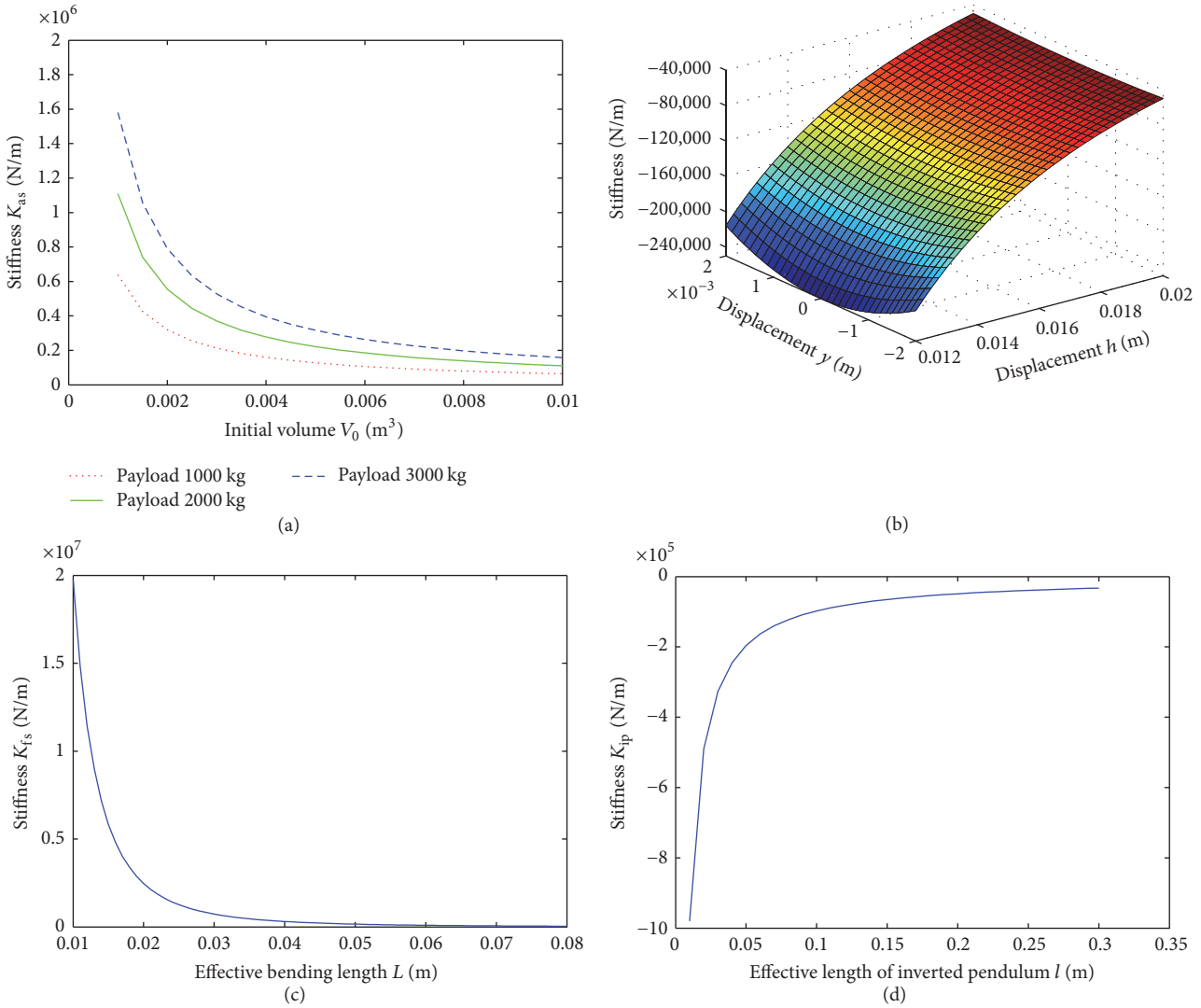

FIGURE 9: The simulation curves, (a) the relationship between stiffness K_{as} of the PS air spring and the initial volume V_0 of the air chamber under different payload mass (M_p = 1000, 2000, and 3000 kg), (b) the stiffness K_{ms} of the NS magnetic spring with the following magnet parameters: the upper/lower 35 mm × 14 mm × 7 mm, the middle 30 mm × 10 mm × 10 mm, $B_r = J = 1.34T$, a relative permeability μ_o, equal to 1.023, (c) the relationship between stiffness K_{fs} of the PS flat spring and the effective bending length L of the flat spring, with the bending section moment of inertia ($I = 2.193e-5$ kg·m^2) being constant, and (d) the relationship between stiffness K_{ip} of the NS inverted pendulum and the effective length of inverted pendulum l, with the payload mass (m = 1000 kg) being constant. Other unknown parameters are shown in Tables 1 and 2.

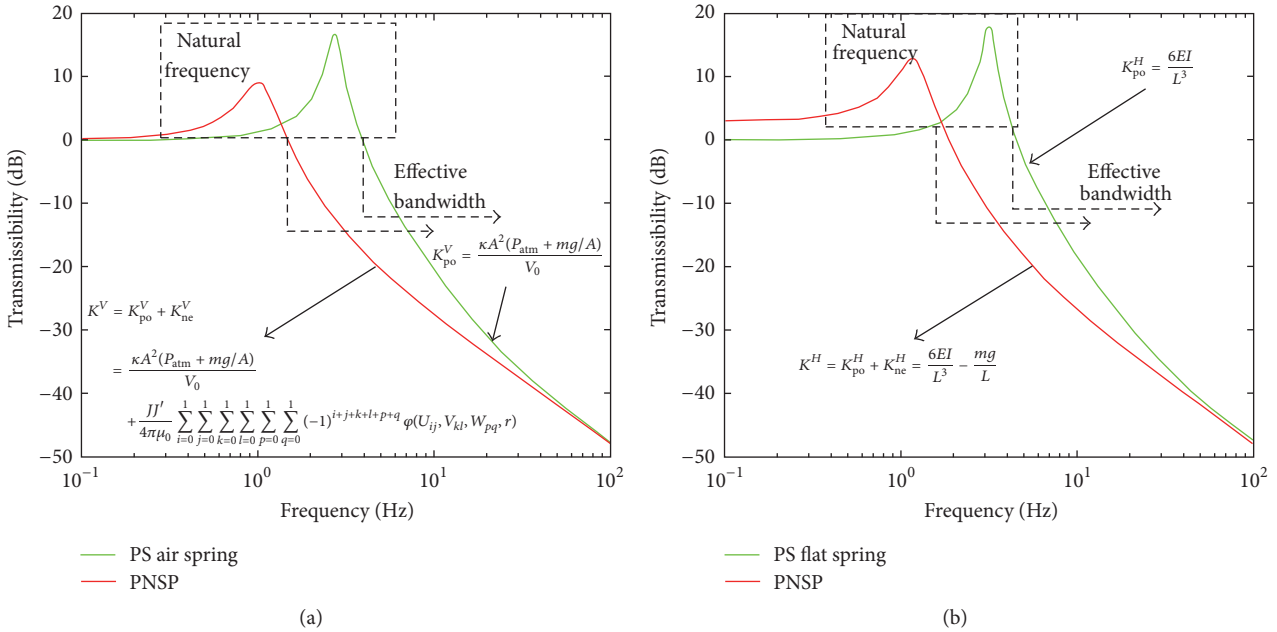

FIGURE 10: Transmissibility curves of different stiffness model, (a) vertical direction; (b) horizontal direction.

According to the simulation parameters of Tables 1 and 2, the transmissibility curves of vibration isolation system are, respectively, shown in Figure 10.

From Figure 10(a), it can be seen that there are obvious differences under different methods in vertical direction. Where the green curve is the transmissibility curve of adopting positive stiffness element alone, the red line is the transmissibility curve of using PNSP. From the result, it can be seen clearly that the natural frequency with PNSP is moved forward; effective bandwidth of vibration isolation is widened.

According to the above theoretical analysis of horizontal direction, Figure 10(b) shows the transmissibility curves under different methods. Where the green curve is the transmissibility curve of adopting positive stiffness element alone, the red line is the transmissibility curve of using PNSP. From the result, we can clearly get that the natural frequency with PNSP is moved forward; effective bandwidth of vibration isolation is widened.

5. Experimental Results and Discussions

5.1. Principle Diagram and Layout of Experiment System. In order to verify the effectiveness of the proposed structure, the principle diagram shown in Figure 11(a) is set up. The vibration isolation system consists of a payload platform, a base platform, three identical vibration isolators, and a real-time position control system and a spectrum testing and analysis system. Two kinds of vibration isolator with different structures (PNSP or PS only) are adopted, respectively, for comparing results. A real-time position control system and a spectrum testing and analysis system (LMS SCADAS) are included in the experiment system. Sensor signals from base platform and payload platform are imported into LMS SCADAS to compare the performance of the vibration isolator with PNSP or PS structure. In the position control loop,

TABLE 1: Simulation parameters of vertical direction.

Parameters	Name	Values
M_p	The mass of payload	1000 kg
A	The effective sectional area of the air chamber	0.0343 m^2
V_0	The initial volume of the air chamber	0.002 m^3
κ	The adiabatic coefficient	1.402
P_{atm}	The pressure of atmosphere	101.325 kpa
a	The dimension of the upper/lower magnets (length)	0.035 m
b	The dimension of the upper/lower magnets (width)	0.014 m
c	The dimension of the upper/lower magnets (height)	0.007 m
a'	The dimension of the middle magnet (length)	0.030 m
b'	The dimension of the middle magnet (width)	0.010 m
c'	The dimension of the middle magnet (height)	0.010 m
h	The distance between the magnets	0.012 m
K^V_{po}	The positive stiffness of vertical direction	3.09e5 N/m
K^V_{ne}	The negative stiffness of vertical direction	−2.52e5 N/m
K^V	The system stiffness of vertical direction	5.68e4 N/m

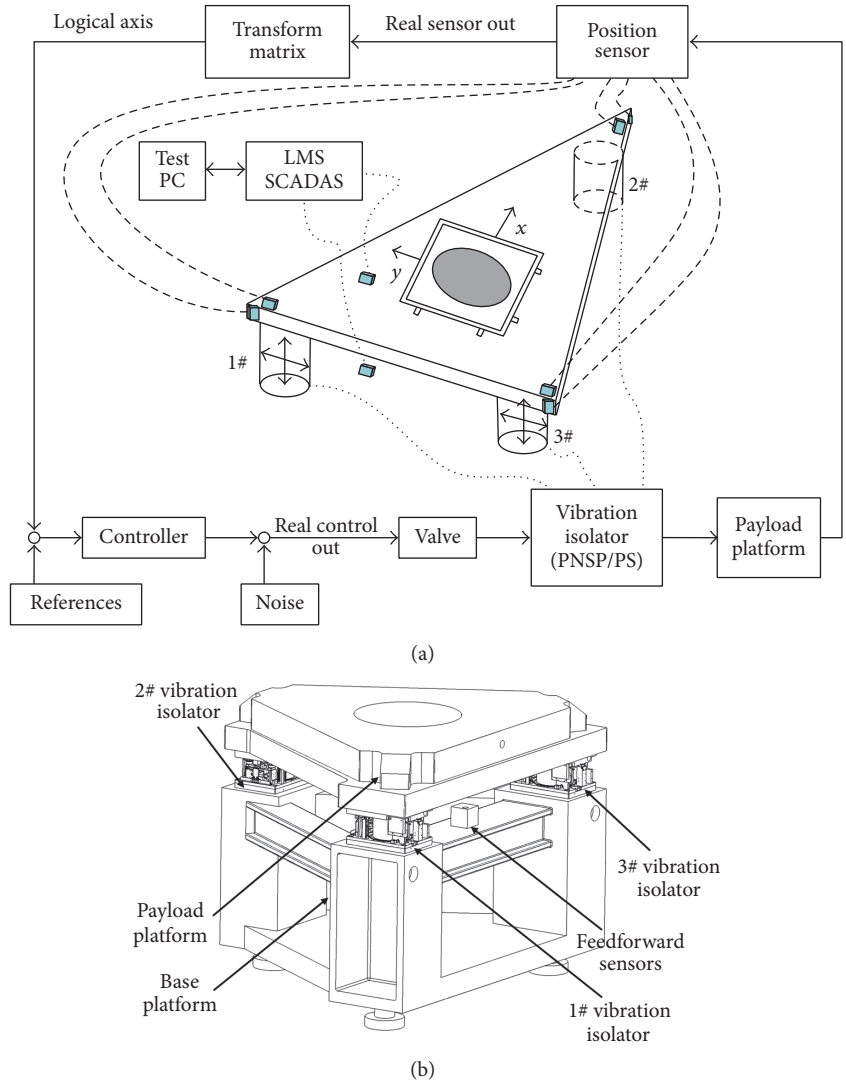

Figure 11: The layout of the ultra-precision vibration isolation system.

the six displacements from horizontal and vertical sensors are converted to the logical axis signals by means of a transform matrix firstly. The error between the setting value of air spring floating and logical axis signal is input to the controller for position control. The output control signal is sent to the valve to control the vibration isolator with PNSP or PS structure and consequently realize the position control of the payload platform.

The vibration isolators which are as isosceles triangle or equilateral triangle arrangement are installed on the base platform. The payload platform and the vibration isolators are fixed and connected with each other through screws. The layout of the ultra-precision vibration isolation system is shown in Figure 11(b).

5.2. Set-Up of Experiments. According to the principle of Figure 11(a), an experiment on the proposed isolator with PNSP structure as Figure 12 is built in super-clean lab. The experiment system consists of three vibration isolators which are as equilateral triangle arrangement installed on the base platform and a control system which can realize real-time position control and fast spectrum test and analysis.

The real-time active control system proposed in paper consists of a programmable NI controller (Model: PXIE-8135) and a control cubicle. It is used as a real-time signal acquisition and a real-time active control signal output. The spectrum testing and analysis system proposed in paper consists of two servo velocity meters (Model: VSE-15D6) and a vibration signal collecting and analysis instrument (Model: LMS SCADASIII SCM05). The vibration signal acquired by the servo velocity meter is sent to the LMS SCADASIII for data processing.

5.3. Experiment Results. The velocity admittance curves of vibration isolation system in the logical axis coordinates are tested to verify the effect of the proposed PNSP structure. The experiment results are shown in Figure 13 and Table 3. From the results, we can see that the natural frequency of X

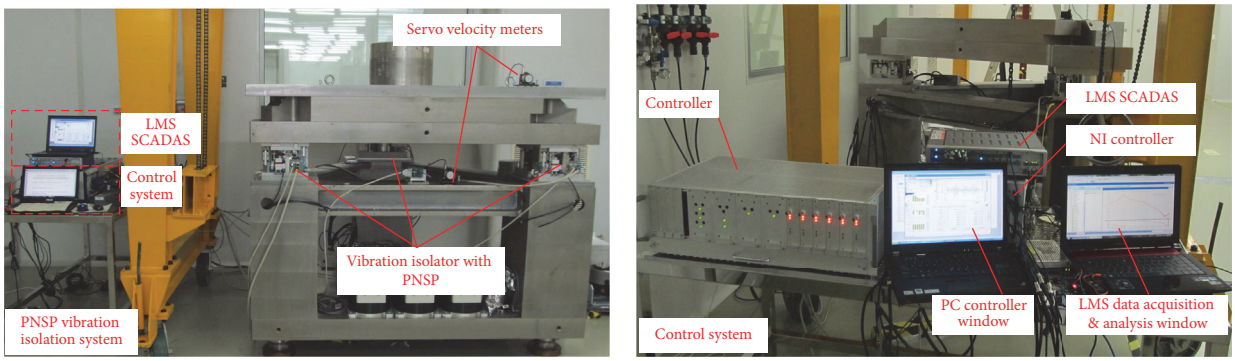

(a) (b)

Figure 12: The experimental system, (a) the principle diagram; (b) the photo of the PNSP vibration isolation system.

Table 2: Simulation parameters of horizontal direction.

Parameters	Name	Values
E	The elastic modulus of flat spring material	2.06e11 Pa
I	The bending section moment of inertia	2.193e – 5 kg∗m^2
L	The effective bending length of the flat spring	0.074 m
m	The equivalent mass of inverted pendulum	1000 kg
l	The effective length of inverted pendulum	0.032 m
K^V_{po}	The positive stiffness of vertical direction	1.29e5 N/m
K^V_{ne}	The negative stiffness of vertical direction	−8.17e4 N/m
K^V	The system stiffness of vertical direction	4.77e4 N/m

Table 3: The natural frequency comparison of vibration isolator using different structure.

Natural frequency	X	Y	Rz	Z	Ry	Rx
PS	2.86 Hz	3.36 Hz	4.37 Hz	2.69 Hz	2.41 Hz	6.64 Hz
PNSP	1.17 Hz	1.19 Hz	1.94 Hz	1.13 Hz	0.98 Hz	1.95 Hz

translation is reduced from 2.86 Hz (PS) to 1.17 Hz (PNSP), the natural frequency of Y translation is reduced from 3.36 Hz (PS) to 1.19 Hz (PNSP), the natural frequency of Z rotation is reduced from 4.37 Hz (PS) to 1.94 Hz (PNSP), the natural frequency of Z translation is reduced from 2.69 Hz (PS) to 1.13 Hz (PNSP), the natural frequency of Y rotation is reduced from 2.41 Hz (PS) to 0.98 Hz (PNSP), and the natural frequency of X rotation is reduced from 6.54 Hz (PS) to 1.95 Hz (PNSP). It can be seen that the natural frequency of each DOF has a substantial decline. Besides above, there is a coupling peak in the direction of X translation due to inadequate decoupling. The second resonance peak maybe is the natural frequency of X rotation. However, compared with the PS, the PNSP still can significantly reduce the natural frequency of the system.

Figure 14 shows the analytical and experimental results of acceleration vibration transmission of the vibration isolator due to oscillation of the vibration isolation system. Tables 4 and 5 list the natural frequency and magnitude of vibration transmissibility curves in different directions separately. The analytical results are calculated by (18) and (28) without regard to the damping of vibration isolation system. PS (green solid line) means that the vibration isolation system only uses positive stiffness mechanism. PNSP (red solid line) means that the vibration isolation system adopts positive stiffness mechanism and negative stiffness mechanism together.

In Figure 14(a) and Tables 4 and 5, because of the low-dynamic stiffness of PNSP structure in the direction of X, the frequency of the resonance peak is moved from 2.79 Hz (PS, error 0.36%) to 1.17 Hz (PNSP, error 1.74%). In the 2.79 Hz, the amplitude of the red solid line is −10.99 dB, compared with 18.34 dB of the green solid line; it drops by 29.33 dB. In the 10 Hz, the amplitude is also from −18.61 dB of the green solid line to −31.90 dB of the red solid line; it drops by 13.29 dB.

In Figure 14(b) and Tables 4 and 5, because of the low-dynamic stiffness of PNSP structure in the direction of Y, the frequency of the resonance peak is moved from 3.32 Hz (PS, error 0.91%) to 1.21 Hz (PNSP, error 0.83%). In the 3.32 Hz, the amplitude of the red solid line is −11.45 dB, compared with 18.36 dB of the green solid line; it drops by 19.48 dB. In the 10 Hz, the amplitude is also from −14.65 dB of the green solid line to −31.44 dB of the red solid line; it drops by 16.79 dB.

In Figure 14(c) and Tables 4 and 5, because of the low-dynamic stiffness of PNSP structure in the direction of Z, the frequency of the resonance peak is moved from 2.75 Hz (PS, error 1.79%) to 1.14 Hz (PNSP, error 3.64%). In the 2.75 Hz, the amplitude of the red solid line is −10.59 dB, compared with 16.78 dB of the green solid line; it drops by 27.37 dB. In the 10 Hz, the amplitude is also from −18.24 dB of the green solid line into −34.78 dB of the red solid line; it drops by 16.54 dB.

In order to further verify the high-static stiffness characteristics of PNSP structure and the stability of the payload

Table 4: The natural frequency of vibration transmissibility curves in different directions.

Direction	PS frequency (Calculation)	PS frequency (Experiment)	Error (%)	PNSP frequency (Calculation)	PNSP frequency (Experiment)	Error (%)
X	2.80 Hz	2.79 Hz	0.36	1.15 Hz	1.17 Hz	1.74
Y	3.30 Hz	3.32 Hz	0.91	1.20 Hz	1.21 Hz	0.83
Z	2.80 Hz	2.75 Hz	1.79	1.10 Hz	1.14 Hz	3.64

Table 5: The magnitude of vibration transmissibility curves in different directions.

Direction	Frequency	PS magnitude (Experiment)	PNSP magnitude (Experiment)	Decreasing amplitude PS resonance/10 Hz
X	PS resonance/10 Hz	18.34 dB/−18.61 dB	−10.99 dB/−31.90 dB	29.33dB/13.29 dB
Y	PS resonance/10 Hz	18.36 dB/−14.65 dB	−11.45 dB/−31.44 dB	19.48dB/16.79 dB
Z	PS resonance/10 Hz	16.78 dB/−18.24 dB	−10.59 dB/−34.78 dB	27.37dB/16.54 dB

Table 6: The static stability of payload platform.

Static stability	$H1$	$H2$	$H3$	$V1$	$V2$	$V3$
Positive deviation (+)	2.5 μm	1.0 μm	2.0 μm	2.0 μm	1.0 μm	2.0 μm
Negative deviation (−)	3.0 μm	1.5 μm	2.0 μm	2.5 μm	1.0 μm	1.5 μm

platform, six eddy current displacement sensor signals are collected, respectively. The working position of the air spring is set up to 1700 μm. When the system is floating up to the working position, three displacement values in the horizontal and vertical physical axis are measured and recorded by the sensors. The experiment results are given in Figure 15 and Table 6.

Table 6 shows that the static stability of the payload platform can be kept within ±3.0 μm and is less than the active positioning accuracy (8 μm, 4 μm, and 15 μm) with different control algorithms in [20]. Despite decreasing of the dynamic stiffness of the vibration isolation system, the static stiffness is preserved and the system stability is still guaranteed. The horizontal deviation and vertical deviation of 2# vibration isolator are better than those of 1# and 3# in the static stability of the payload platform. This result may be attributed to the problems that the centroid of the isosceles structure is far from 2# isolator.

5.4. Discussions. On the condition of the open loop, compared to the PS vibration isolator, the PNSP vibration isolator plays an important role in reducing the dynamic stiffness and preserving the static stiffness of the system. From the experimental results of velocity admittance curves, the natural frequency of Z translation is reduced from 2.69 Hz of PS to 1.13 Hz of PNSP, and the six directions of the system are significantly decreased. The comparison results of the vibration transmissibility curves show that the vibration transmissibility of the new system is improved obviously with employing the PNSP structure. The results are basically the same with the results of the simulation. It also can be judged from the stability experiment of the system simultaneously. The dynamic stiffness of the system is still preserved, and the stability of the system is well guaranteed.

The above-mentioned experimental results illustrate that the PNSP vibration isolator can effectively reduce the natural frequency of the system and further expand the ultra-low frequency of vibration isolation system. At the same time, it also provides the foundation for the further enhancement of the vibration attenuation ability in active control.

6. Conclusion

A compact structure with PNSP is designed to reduce the natural frequency and broaden the effective bandwidth of vibration isolation system according to the principle of high-static-low-dynamic stiffness. The proposed isolator combines a PS spring with a NS spring in parallel in two DOFs of horizontal and vertical direction. Different stiffness models of PS elements and NS elements for vertical and horizontal directions are established. And three identical vibration isolators can be used together to establish an ultra-low frequency vibration isolation system, which can realize the ultra-low frequency vibration isolation in six degrees of freedom. A real-time active control system and a spectrum testing and analysis system are employed for contrast experiment between the proposed PNSP structure and PS structure. The velocity admittance results demonstrate that the natural frequency of Z translation is reduced from 2.69 Hz of PS to 1.13 Hz of PNSP. The transmissibility curves also prove that the frequency of the resonance peak is moved forward 1.61 Hz (from 2.75 Hz to1.14 Hz). In 2.75 Hz, the amplitude drops by 27.37 dB. In the 10 Hz, the amplitude drops by 16.54 dB. The static stability of the payload platform can be kept within ±3.0 μm and is less than the active positioning accuracy (8 μm, 4 μm, and 15 μm). It means that PS with NS in parallel can obviously reduce the natural frequency and broaden the effective bandwidth of the system and simultaneously maintain the stability of the system and further verify the validity and superiority of the mentioned structure. Consequently,

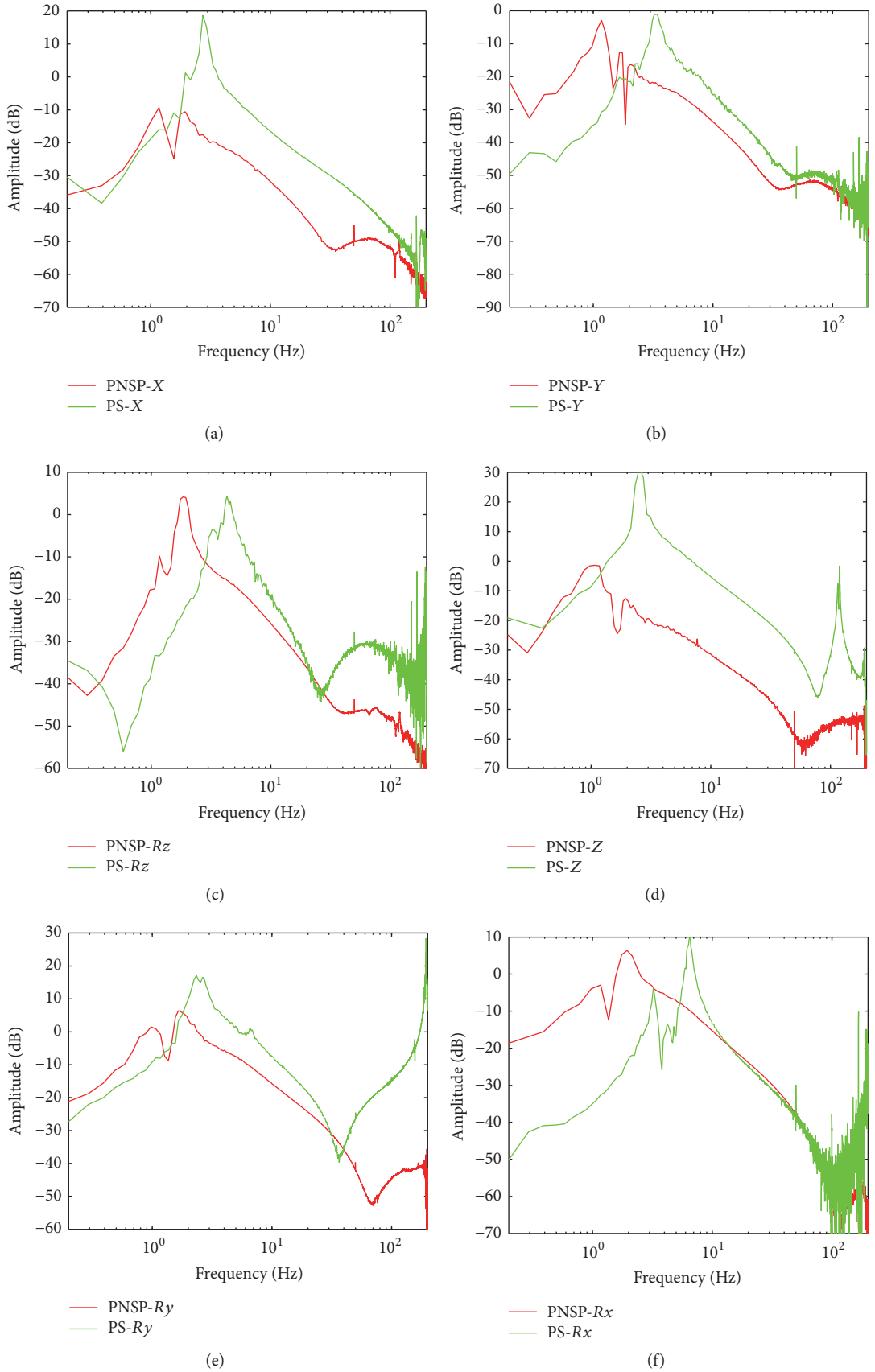

Figure 13: The velocity admittance curves of logical axes (the red solid line for PNSP and the green solid line for PS), (a) X translation, (b) Y translation, (c), Z rotation, (d) Z translation, (e) Y rotation, and (f) X rotation.

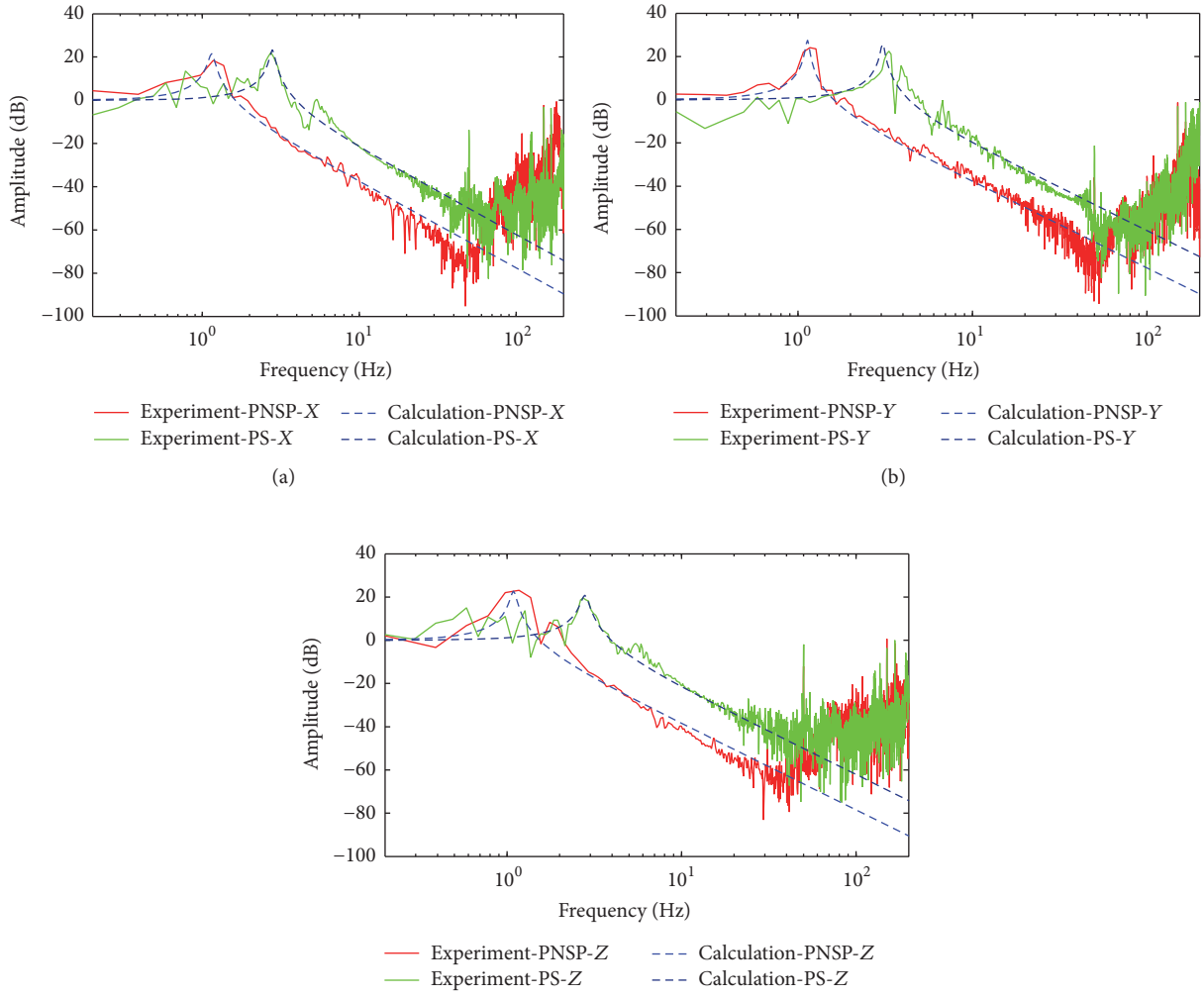

FIGURE 14: The vibration transmissibility curves (the red solid line for PNSP, the green solid line for PS), (a) X translation, (b) Y translation, and (c) Z translation.

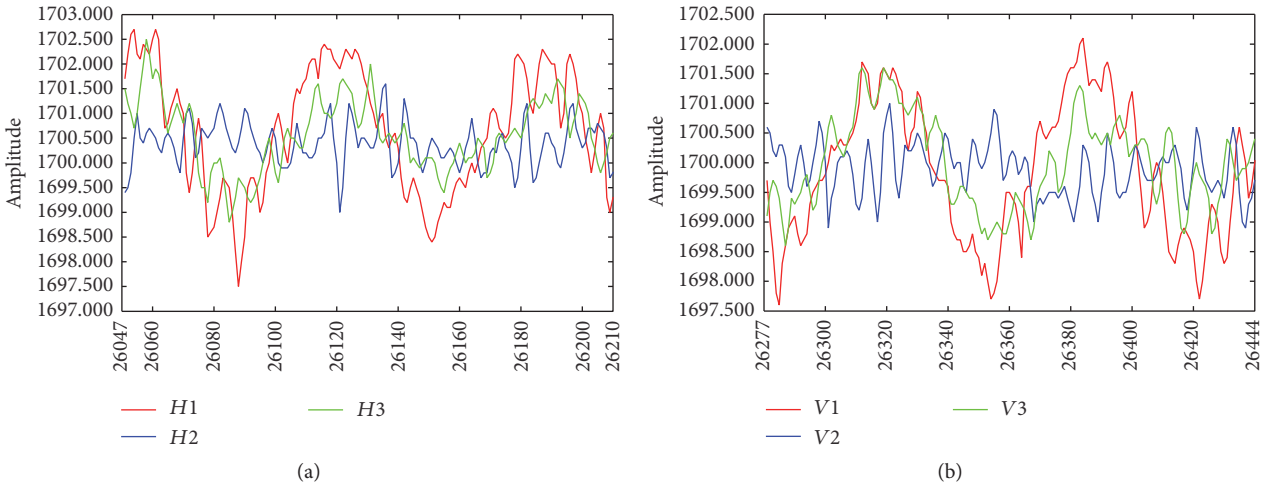

FIGURE 15: The static stability of payload platform, (a) the horizontal displacement; (b) the vertical displacement.

this type of vibration isolator is suitable for applications on ultra-precision manufacturing and measurement equipment.

Competing Interests

The authors declare that there is no conflict of interests regarding the publication of this paper.

Acknowledgments

The work was supported by the National Natural Science Foundation of China (no. 51435006, no. 51421062).

References

[1] C. G. Gordon, "Generic vibration vriteria for vibration-sensitive equipment," in *Proceedings of the International Society for Optical Engineering (SPIE) Conference on Current Developments in Vibration Control for Optomechanical Systems*, E. A. Derby, Ed., International Society for Optics and Photonics, pp. 22–33, Denver, Colo, USA, July 1999.

[2] E. H. Anderson and B. Houghton, "ELITE-3 active vibration isolation workstation," in *Proceedings of the 8th Annual International Symposium on Smart Structures and Materials*, pp. 183–196, International Society for Optics and Photonics, March 2001.

[3] Y.-H. Shin and K.-J. Kim, "Performance enhancement of pneumatic vibration isolation tables in low frequency range by time delay control," *Journal of Sound and Vibration*, vol. 321, no. 3–5, pp. 537–553, 2009.

[4] S. Julai and M. Tokhi, "Active vibration control of flexible plate structures with distributed disturbances," *Journal of Low Frequency Noise Vibration and Active Control*, vol. 31, no. 2, pp. 123–150, 2012.

[5] B. Yan, M. J. Brennan, S. J. Elliott, and N. S. Ferguson, "Active vibration isolation of a system with a distributed parameter isolator using absolute velocity feedback control," *Journal of Sound and Vibration*, vol. 329, no. 10, pp. 1601–1614, 2010.

[6] M. Yasuda, T. Osaka, and M. Ikeda, "Feedforward control of a vibration isolation system for disturbance suppression," in *Proceedings of the 35th IEEE Conference on Decision and Control*, pp. 1229–1233, Kobe, Japan, December 1996.

[7] T. H. Yan, H. Y. Pu, X. D. Chen, Q. Li, and C. Xu, "Integrated hybrid vibration isolator with feedforward compensation for fast high-precision positioning X/Y tables," *Measurement Science and Technology*, vol. 21, no. 6, Article ID 065901, 10 pages, 2010.

[8] D. L. Platus, "Negative-stiffness-mechanism Vibration Isolation Systems," in *Proceedings of the SPIE's International Symposium on Optical Science, Engineering, and Instrumentation*, International Society for Optics and Photonics, pp. 98–105, 1999.

[9] B. A. Fulcher, D. W. Shahan, M. R. Haberman, C. C. Seepersad, and P. S. Wilson, "Analytical and experimental investigation of buckled beams as negative stiffness elements for passive vibration and shock isolation systems," *Journal of Vibration and Acoustics*, vol. 136, no. 3, Article ID 031009, 12 pages, 2014.

[10] M. E. Hoque, T. Mizuno, Y. Ishino, and M. Takasaki, "A three-axis vibration isolation system using modified zero-power controller with parallel mechanism technique," *Mechatronics*, vol. 21, no. 6, pp. 1055–1062, 2011.

[11] T. Mizuno, M. Takasaki, D. Kishita, and K. Hirakawa, "Vibration isolation system combining zero-power magnetic suspension with springs," *Control Engineering Practice*, vol. 15, no. 2, pp. 187–196, 2007.

[12] W. S. Robertson, M. R. F. Kidner, B. S. Cazzolato, and A. C. Zander, "Theoretical design parameters for a quasi-zero stiffness magnetic spring for vibration isolation," *Journal of Sound and Vibration*, vol. 326, no. 1-2, pp. 88–103, 2009.

[13] A. Valeev, A. Zotov, and S. Kharisov, "Designing of compact low frequency vibration isolator with quasi-zero-stiffness," *Journal of Low Frequency Noise Vibration and Active Control*, vol. 34, no. 4, pp. 459–474, 2015.

[14] A. Carrella, M. J. Brennan, and T. P. Waters, "Static analysis of a passive vibration isolator with quasi-zero-stiffness characteristic," *Journal of Sound and Vibration*, vol. 301, no. 3, pp. 678–689, 2007.

[15] P. Alabuzhev, A. Gritchin, L. Kim, G. Migirenko, V. Chon, and P. Stepanov, *Vibration Protecting and Measuring Systems with Quasi-Zero Stiffness*, CRC Press Hemisphere, New York, NY, USA, 1989.

[16] A. Carrella, M. J. Brennan, T. P. Waters, and K. Shin, "On the design of a high-static-low-dynamic stiffness isolator using linear mechanical springs and magnets," *Journal of Sound and Vibration*, vol. 315, no. 3, pp. 712–720, 2008.

[17] A. D. Shaw, S. A. Neild, and D. J. Wagg, "Dynamic analysis of high static low dynamic stiffness vibration isolation mounts," *Journal of Sound and Vibration*, vol. 332, no. 6, pp. 1437–1455, 2013.

[18] W. Wu, X. Chen, and Y. Shan, "Analysis and experiment of a vibration isolator using a novel magnetic spring with negative stiffness," *Journal of Sound and Vibration*, vol. 333, no. 13, pp. 2958–2970, 2014.

[19] G. Akoun and J.-P. Yonnet, "3D analytical calculation of the forces exerted between two cuboidal magnets," *IEEE Transactions on Magnetics*, vol. 20, no. 5, pp. 1962–1964, 1984.

[20] T. H. Lee, K. K. Tan, S. N. Huang, and H. F. Dou, "Intelligent control of precision linear actuators," *Engineering Applications of Artificial Intelligence*, vol. 13, no. 6, pp. 671–684, 2000.